Numerical Calculation of Three-Dimensional Turbulent Flow in Compound Rectangular Open Channels

by

Dan NAOT*, Iehisa NEZU**, and Hiroji NAKAGAWA**

(Received December 5, 1991)

Abstract

The hydrodynamic response of the turbulent flow in a compound rectangular open channel to the flood plain depth, roughness, and symmetry and to the channel Reynolds number was demonstrated. The flow in the four basic asymmetric channels measured by Tominaga and Nezu (1991) was numerically simulated, as well as other channel configurations including symmetric channels. Turbulence was modeled by the energy dissipation model, combined with the algebraic stress model suggested by Naot and Rodi (1982). The three-dimensional flow with secondary currents in compound open channels was solved numerically using the parabolic pressure correction algorithm of Patankar and Spalding (1972). The examples suggest data bases for the estimation of friction factors, and for the mass exchange rate between the flood plain interior and its threshold. A possible explanation for the multi-cellular structure in wide open channels is also given.

1. INTRODUCTION

With the advance of computing methods, it has become possible to obtain, at a reasonable cost, numerical calculations for three-dimensional turbulent flow with secondary currents driven by the interactions of the turbulent eddies with the free surface, with the geometry of the channel, and with the roughness heterogeneity along the wetted perimeter. In this study, the hydrodynamic behaviour of the compound rectangular open channels is illustrated.

The early calculations of turbulent square duct flow with secondary currents, performed by Launder and Ying (1973), were followed by conservative calculation of the full Reynolds stress model equations of Naot, Shavit and Wolfshtein (1974), and Reece (1976), and also by algebraic presentation of the turbulent stresses incorporated in an energy dissipation model used by Tatchel (1975), Gessner and Emergy (1979), Neti and Eichhorn (1979)

* Center for Technological Education, P. O. Box 305, Holon 58102, ISRAEL
** Division of Global Environment Engineering, Graduate School of Engineering Kyoto University, Kyoto 606, JAPAN

and many others. More detailed information about the turbulence-driven secondary currents in channel flows are given in the IAHR-monograph written by Nezu & Nakagawa (1992).

To adjust the open channel flow it is necessary to note that adjacent to the free surface the turbulent eddies do not have sufficient energy to project above the free surface. Thus, the eddies break down to smaller ones and the velocity fluctuations are redistributed there. These two additional interactions induced by the free surface were first modeled by Reece (1976), who used a full Reynolds stress model. Naot and Rodi (1982) demonstrated the use of an algebraic stress model for the calculation of secondary currents, turbulence energy and dissipation scale, and for the local wall shear stress in turbulent open channel flow. The comparison of the calculations with the experimental data measured by Nezu and Rodi (1985) with a laser Doppler anemometer in open channels showed a reasonable agreement approving this simplification.

The present study is devoted to the hydrodynamic behaviour of the compound rectangular open channel. The calculations show pairs of longitudinal vortices at the corners of the rectangular flood plain and the rectangular main channel similar in strength and structure to those found in a single rectangular open channel by Naot and Rodi (1982). In addition, however, at the flood plain threshold, an intensive vortex pair was experimentally shown by Tominaga, Nezu and Kobatake (1989), and Tominaga and Nezu (1991), with one vortex at the flood plain threshold and the second one at the main channel. The accurate prediction of this vortex pair is a necessary condition for the determination of the continuous mass and sediment exchange between the two sub channels.

To accomplish this task, an accurate estimation of the mass exchange rate between the two vortices is needed. Flow visualization (e. g., Tamai, Asaeda and Ikeda, 1986) suggests that these vortices are related by a special type of coherent suructure. Although this effect was not modeled, the results for the mean velocity field are plausible, suggesting that the effect is mainly important for sediments exchange and is of lesser importance for the ambient fluid.

Finally, recent experiments in urban open channels by Nezu and Nakagawa (1991) show multi-cellular structure that is substantially more intensive than that found in sand free laboratory open channels by Imamoto, Ishigaki and Nishida (1989). A possible explanation for this behaviour is also suggested.

2. THE HYDRODYNAMIC MODEL

The set of equations solved for the turbulent flow in the compound open channel shown in Fig. 1 consists of three groups of equations that together form a well-defined closed parabolic system. The groups are : three momentum equations plus the continuity equation

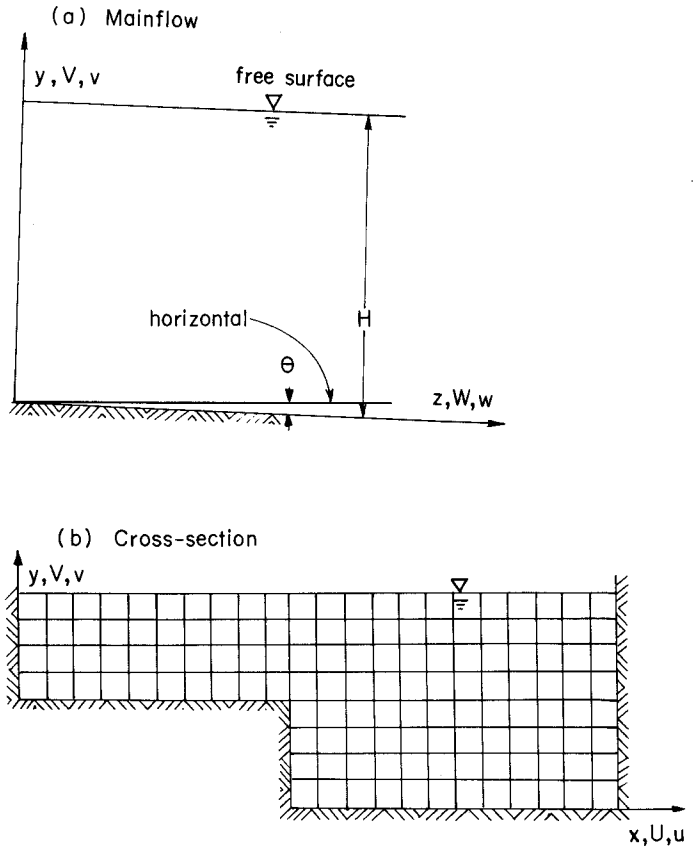

Fig. 1 The Compound Open-Channel Coordinate System.

governing the three-dimensional mean motion and the mean pressure; two transport equations for the energy of turbulence and the dissipation representing the amplitude and scale of the turbulent velocity fluctuations; and six algebraic equations representing the anisotropy by means of the Reynolds stresses, given in terms of the turbulence energy, k, dissipation, ε, and the mean velocity gradients, $\partial U_i/\partial x_j$. The model coefficients are those recommended by Naot and Rodi (1982) with some modifications discussed in the following.

2.1 The Mean Velocities

This set contains the continuity equation:

$$\frac{\partial U}{\partial x}+\frac{\partial V}{\partial y}+\frac{\partial W}{\partial z}=0 \tag{1}$$

and three momentum equations:

$$U\frac{\partial W}{\partial x}+V\frac{\partial W}{\partial y}+W\frac{\partial W}{\partial z}=-\frac{1}{\rho}\frac{\partial \phi^*}{\partial z}-\frac{\partial}{\partial y}(\overline{vw})-\frac{\partial}{\partial x}(\overline{uw}) \tag{2}$$

$$U\frac{\partial U}{\partial x}+V\frac{\partial U}{\partial y}+W\frac{\partial U}{\partial z}=-\frac{1}{\rho}\frac{\partial \phi}{\partial x}-\frac{\partial}{\partial y}(\overline{uv})-\frac{\partial}{\partial x}(\overline{u^2}) \tag{3}$$

and

$$U\frac{\partial V}{\partial x}+V\frac{\partial V}{\partial y}+W\frac{\partial V}{\partial z}=-\frac{1}{\rho}\frac{\partial \phi}{\partial y}-\frac{\partial}{\partial y}(\overline{v^2})-\frac{\partial}{\partial x}(\overline{uv}) \tag{4}.$$

In these equations, the viscous terms can be neglected at high Reynolds numbers.

The pressure gradient components and the gravity forces were replaced in Equations (3) and (4) by a scalar ϕ

$$\phi=P-P_{atm}-\rho g\cos\theta\cdot(H(z)-y) \tag{5}$$

representing deviations from the hydrostatic pressure, and by another scalar ϕ^* in Equation (2)

$$\frac{1}{\rho}\frac{\partial \phi^*}{\partial z}=\frac{1}{\rho}\frac{\partial \phi}{\partial z}-gI_e \tag{6}$$

where, $I_e\equiv\sin\theta-\cos\theta\cdot dH/dz$

representing streamwise motivating forces, with no loss of generality. The term I_e is the energy gradient. However, to use the Patankar and Spalding (1972) algorithm, it is necessary to assume that $\partial\phi/\partial z$ appearing in Equation (6) depends on the z coordinate only, thus restricting the calculations to flows with weak lateral motion. Still, the results presented here are exact, as they are restricted to the fully developed situation in which $\partial\phi^*/\partial z$ becomes constant and equal to $-\rho g\sin\theta$; the condition of the uniform normal flow, i. e., $dH/dz=0$.

The assumption that $\partial\phi/\partial z$ can be replaced by a typical function of z (which is independent of x and y) is very important from the computational point of view. The main outcome of such an assumption is the ability to separate the calculation of $\partial\phi^*/\partial z$ from the calculation of $\partial\phi/\partial x$ and $\partial\phi/\partial y$. The Spalding–Patanker (1972) algorithm applies global continuity considerations to the calculation of the first and local considerations to the second. It derives $\partial\phi^*/\partial z$ from the condition for conservation of the total mass flow through the channel, and derives both $\partial\phi/\partial x$ and $\partial\phi/\partial y$ from local continuity conservation using the pressure correction technique.

Once $\partial\phi^*/\partial z$ is calculated, the problem of how to split it among the two parts of Equation (6) still remains. Being interested in results for a fully developed flow, one may write

$\partial\phi/\partial z=0$, $dH/dz=0$, and use $\partial\phi^*/\partial z$ to calculate the inclination angle, θ.

2.2 The Energy-Dissipation ($k-\varepsilon$) Turbulence Model

The energy-dissipation turbulence model consists of two transport equations for the turbulent energy, k:

$$U\frac{\partial k}{\partial x}+V\frac{\partial k}{\partial y}+W\frac{\partial k}{\partial z}=\frac{\partial}{\partial x}\left(\frac{\nu_{tx}}{\sigma_k}\frac{\partial k}{\partial x}\right)+\frac{\partial}{\partial y}\left(\frac{\nu_{ty}}{\sigma_k}\frac{\partial k}{\partial y}\right)+G-\varepsilon \tag{7}$$

and for the dissipation, ε :

$$U\frac{\partial \varepsilon}{\partial x}+V\frac{\partial \varepsilon}{\partial y}+W\frac{\partial \varepsilon}{\partial z}=\frac{\partial}{\partial x}\left(\frac{\nu_{tx}}{\sigma_\varepsilon}\frac{\partial \varepsilon}{\partial x}\right)+\frac{\partial}{\partial y}\left(\frac{\nu_{ty}}{\sigma_\varepsilon}\frac{\partial \varepsilon}{\partial y}\right)+\frac{\varepsilon}{k}(C_{\varepsilon 1}G-C_{\varepsilon 2}\varepsilon) \tag{8}$$

G is the production or generation of energy by the mean velocity gradients and it is modeled by

$$G=\nu_{tx}\left(\frac{\partial W}{\partial x}\right)^2+\nu_{ty}\left(\frac{\partial W}{\partial y}\right)^2 \tag{9}$$

Equations (7)-(9) contain four model coefficients. The specification of these, in view of the predictability of important features of channel flow, was given by Launder and Spalding (1974). We therefore note only the present choice :

$$C_{\varepsilon 1}=1.44,\ C_{\varepsilon 2}=1.92,\ \sigma_k=1.225 \text{ and } \sigma_\varepsilon=1.225 \tag{10}$$

Away from the free surface, ν_{tx} and ν_{ty} become equal to the scalar turbulent viscosity

$$\nu_t=C_\mu\frac{k^2}{\varepsilon} \qquad (\text{with } C_\mu=0.09) \tag{11}$$

and the model becomes the standard $k-\varepsilon$ model. Near the free surface, however, we must use the corrected anisotropic viscosities, ν_{tx} and ν_{ty}, for the description of both the turbulent transports of the energy, k, and dissipation, ε.

2.3 The Algebraic Stress Model

The algebraic stress model is derived from the full stress transport model assuming local equilibrium, where the production of turbulence balances its dissipation, i. e., $G=\varepsilon$. The suggestion of Launder, Reece, and Rodi (1975) was modified, and a free-surface proximity correction of the pressure-strain correlation of the form suggested by Shir (1973) was added (Naot and Rodi 1982, 1983) :

$$(1-\alpha)G_{ij}-\beta D_{ij}-\gamma k\left(\frac{\partial U_i}{\partial x_j}+\frac{\partial U_j}{\partial x_i}\right)+\frac{2}{3}(\alpha+\beta)G\delta_{ij}-\frac{\varepsilon}{k}\left[\overline{u_iu_j}C_1+\frac{2}{3}k(1-C_1)\delta_{ij}\right]$$
$$-\left(\frac{3}{2}C_3\right)\frac{\varepsilon}{k}\left[\overline{u_nu_i}\delta_{nj}+\overline{u_nu_j}\delta_{ni}-\frac{2}{3}\overline{u_n^2}\delta_{ij}\right]=0 \qquad (12).$$

The index n denotes the unit vector normal to the free surface

$$G_{ij}=-\left(\overline{u_iu_l}\frac{\partial U_j}{\partial x_l}+\overline{u_ju_l}\frac{\partial U_i}{\partial x_l}\right) \qquad (13)$$

$$D_{ij}=-\left(\overline{u_iu_l}\frac{\partial U_l}{\partial x_j}+\overline{u_ju_l}\frac{\partial U_l}{\partial x_i}\right) \qquad (14)$$

and $G=(1/2)\ G_{ii}$=the energy production or generation.

Simple constitutive relations can be derived from Equation (12) by applying two additional approximations. The possibility of using constitutive relations stemming from the solutions for unidirectional flow where all derivatives apart from $\partial W/\partial x$ and $\partial W/\partial y$ vanish for the flow with weak lateral motion was examined by Naot and Rodi (1981). They suggested maintaining the isotropic components in the equations for $\overline{u^2}$, $\overline{v^2}$, and $\overline{uv}$, which are expressed by the scalar eddy viscosity, ν_t. The second type of simplifications made in the equations for $\overline{uw}$ and $\overline{vw}$ were suggested by Naot and Rodi (1983), who examined the exact iterative solutions for unidirectional flow adjacent to a free surface. They suggested replacing the complicated solutions for $\overline{uw}$ and $\overline{vw}$ by the simple constitutive relations given in the following. These two steps led to

$$-\overline{vw}=\nu_{ty}\frac{\partial W}{\partial y} \qquad \text{with } \nu_{ty}\equiv\frac{C_1^2}{\left(C_1+\frac{3}{2}C_3\right)(C_1+2C_3)}\nu_t \qquad (15)$$

$$-\overline{uw}=\nu_{tx}\frac{\partial W}{\partial x} \qquad \text{with } \nu_{tx}\equiv\frac{\left(C_1+\frac{5}{2}C_3\right)}{(C_1+2C_3)}\nu_t \qquad (16)$$

for the main shear stresses, and

$$\overline{v^2}=\frac{k}{(C_1+2C_3)}\left[\frac{2}{3}\left(\alpha-\frac{1}{2}\beta+C_1-1\right)+\frac{\beta}{\varepsilon}\left(\overline{vw}\frac{\partial W}{\partial y}-\overline{uw}\frac{\partial W}{\partial x}\right)\right]-2\nu_t\frac{\partial V}{\partial y} \qquad (17)$$

$$\overline{u^2}=\frac{k}{C_1}\left[\frac{2}{3}\left(\alpha-\frac{1}{2}\beta+C_1-1\right)+\frac{\beta}{\varepsilon}\left(\overline{uw}\frac{\partial W}{\partial x}-\overline{vw}\frac{\partial W}{\partial y}\right)+C_3\frac{\overline{v^2}}{k}\right]-2\nu_t\frac{\partial U}{\partial x} \qquad (18)$$

and

$$\overline{uv}=\frac{\beta}{\left(C_1+\frac{3}{2}C_3\right)}\frac{k}{\varepsilon}\left(\overline{uw}\frac{\partial W}{\partial y}+\overline{vw}\frac{\partial W}{\partial x}\right)-\nu_t\left(\frac{\partial U}{\partial y}+\frac{\partial V}{\partial x}\right) \qquad (19)$$

for the stresses that govern the lateral secondary motion.

To obtain constitutive relations that express surface proximity realistically, the model parameters should be given in terms of two functions accounting for the distance from solid walls, f_1, and free surface, f_2, as follows:

$$\alpha=0.7636-0.06f_1 \tag{20}$$
$$\beta=0.1091+0.06f_1 \tag{21}$$
$$C_1=1.50-0.50f_1, \text{ and} \tag{22}$$
$$C_3=0.10f_2 \tag{23}.$$

Naot and Rodi (1982) suggested the use of quadratic formulas rather than linear ones:

$$f_1=\left(\frac{l}{y_a}\right)^2 \text{ and } f_2=\left(\frac{l}{h_a}\right)^2 \tag{24}.$$

Where, l is the dissipation length defined by

$$l=\left(\frac{C_\mu^{3/4}}{\kappa}\right)\frac{k^{3/2}}{\varepsilon} \tag{25}$$

in which κ is the von Karman constant, i. e., $\kappa=0.41$ given by Nezu & Rodi (1986). y_a and h_a are the root-mean-squared reciprocal distances from the solid walls and free surface, respectively:

$$y_a=\left\langle\frac{1}{y^2}\right\rangle^{-1/2} \text{ and } h_a=\left\langle\frac{1}{(h-y)^2}\right\rangle^{-1/2}+0.3162l \tag{26}.$$

Adjacent to the surfaces, both f_1 and f_2 become equal to 1, since $l\simeq y$ near solid walls, and l is finite near free surfaces. Away from the surfaces, both f_1 and f_2 vanish, due to the quadratic formula and the numerical factor introduced into Equation (26) for h_a.

2. 4 Boundary Conditions at Solid Walls

The wall function technique is used near solid walls in order to reduce the computational effort. The numerical solution is matched with additional information, experimental and theoretical, given in the form of wall functions, e. g., see an IAHR-monograph by Nezu & Nakagawa (1992). Near solid walls, a logarithmic profile for the streamwise velocity is valid:

$$W=\frac{U_*}{\kappa}\ln(E\cdot y^+) \tag{27}.$$

Equation (27) is used to derive iteratively the local friction velocity, U_*, from W_1 at the first grid node:

$$U_*^2=\frac{\Gamma \cdot W_1}{y_1} \qquad \text{with } \Gamma=\nu y_1^+\frac{\kappa}{\ln(E \cdot y_1^+)} \tag{28}$$

For hydraulically smooth walls, E is equal to 9, and for completely rough walls :

$$E=\frac{\exp(\kappa B)}{k_s^+} \tag{29}$$

in which $B=8.5$ (the Nikuradse constant), k_s=the roughness height, and $k_s^+\equiv k_s U_*/\nu$. The transition between these two extreme cases, as measured by Nikuradse (1932), can be given with errors smaller than 10% (Naot and Emrani, 1983) by the correlation :

$$E=\frac{9(1+0.3k_s^+)}{1+20/k_s^+} \tag{30}$$

The adjustment of the method to wall roughness heterogeneity is very simple. At each iteration, E is calculated using the formerly calculated U_* and the local roughness height, k_s. Then, E is used to calculate Γ and to produce a new U_*. Knowing that the lateral velocities, U and V, are relatively weak in comparison to the streamwise component, W, and assuming a logarithmic profile also for this component, one may obtain the lateral shear stress from a similar calculation (Naot and Rodi 1982).

The boundary conditions for k and ε stem from the application of the local equilibrium concept to their transport equations, resulting in

$$k_1=\frac{1}{\sqrt{C_\mu}}U_*^2 \quad \text{and} \quad \varepsilon_1=\frac{1}{\kappa y_1}U_*^3 \tag{31}$$

Thus, the wall roughness directly influences the equation for U_* and indirectly, via U_*, the wall conditions for energy and dissipation.

2.5 Free-Surface Renewal Conditions for Dissipation

For most variables the free surface is only a symmetry plane. A unique variable in this respect is the dissipation for which Hossain and Rodi (1980) suggested

$$\varepsilon_s=\frac{C_\mu^{3/4}}{\kappa}k^{3/2}\left(\frac{1}{y'}+\frac{1}{y^*}\right) \tag{32}$$

in which y' =the distance from a virtual surface (extrapolation) located 0.07H above the real free surface. The addition $1/y^*$, in which y^* =the distance from the nearest bank, was introduced to ensure a smooth transition towards the intersection of the free surface and the banks, by Naot and Rodi (1982). However, in the present study the channel depth is not constant. Hence, an alternative boundary condition that imbeds these features but does not depend directly on the channel depth was used. The surface renewal condition of Yacoub,

Moalem-Maron and Naot (1991) is based on the following assumptions: the turbulent kinetic energy available for the formation of a new surface structure by a typical eddy moving from the flow field interior towards the interface is estimated by $E_a=\frac{1}{2}m\overline{v_n^2}$, where m is the typical eddy mass and v_n is the velocity fluctuation perpendicular to the interface. Assuming the typical eddy to be a perfect sphere of diameter l, this estimation becomes:

$$E_a=\left(\frac{\pi}{12}\frac{\overline{v_n^2}}{k}\right)\rho l^3 k \tag{33}$$

In the present study, the free surface is assumed to remain unbreached. Hence, the rejected eddy carries back into the flow field interior the energy E_a. The formation of an inward energy flux is common to both the vertical gas-liquid interface and the free surface of the channel, where gravity plays an important role:

$$J_k=E_a/\tau\Delta s \tag{34}$$

where, τ is a typical time scale and Δs is a typical surface area.

Assuming that $\tau\simeq l/\sqrt{\overline{v_n^2}}$ and $\Delta s=\pi l^2/4$, Equation (34) becomes:

$$J_k=\frac{1}{3}\left(\frac{\overline{v_n^2}}{k}\right)^{3/2}\rho k^{3/2} \tag{35}$$

With the inward energy flux being equal to the outward energy flux, the interface is energetically insulated:

$$dk/dx_n=0 \tag{36}$$

However, owing to the free surface dynamics, the rejected eddies are correlated with the incoming eddies. Thus, when compared with a symmetry layer, the interface induces coherence and a higher collision density is expected in the liquid phase interior (Naot and Rodi 1983).

To enhance dissipation in addition to that expected adjacent to a symmetry layer, one may pose at the boundary a '*dissipation flux*' condition. It is suggested to pose

$$\frac{\nu_t}{\sigma_\varepsilon}\frac{d\varepsilon}{dx_n}=\frac{J_k}{\rho\tau} \tag{37}$$

and relate the dissipation flux to the inward energy flux doomed to dissipate owing to '*wrong timing*':

$$\frac{\nu_t}{\sigma_\varepsilon}\frac{d\varepsilon}{dx_n}=\frac{1}{3}\left(\frac{\overline{v_n^2}}{k}\right)^2\frac{k^2}{l} \tag{38}$$

Using the high-Reynolds-number approximations for the dissipation diffusivity and length, Equation (38) becomes a boundary condition for the dissipation,

$$\frac{d\varepsilon}{dx_n}=C_{\varepsilon F}\frac{\varepsilon^2}{k^{3/2}} \qquad \text{with } C_{\varepsilon F}\equiv\frac{1}{3}\left(\frac{\overline{v_n^2}}{k}\right)^2\frac{\sigma_\varepsilon\kappa}{C_\mu^{7/4}} \tag{39}$$

or an alternative boundary condition for the length,

$$\frac{dl}{dx_n}=-C_{lF} \qquad \text{with } C_{lF}\equiv\frac{1}{3}\left(\frac{\overline{v_n^2}}{k}\right)^2\frac{\sigma_\varepsilon}{C_\mu} \tag{40}$$

Hossain and Rodi's (1980) condition for open-channel flow,

$$l=1.07\mathrm{H}-x_n \tag{41}$$

was so far interpreted as $l=0.07\mathrm{H}$ at $x_n=\mathrm{H}$. However, with the alternative interpretation as $dl/dx_n=-1$, identified as a special case with $C_{lF}=1$ and $\overline{v_n^2}/k=0.456$, the consistent value of $C_{\varepsilon F}$ becomes 2.43. Numerical calculation of one-dimensional open-channel flow showed that the use of $C_{\varepsilon F}=2.43$ is indeed a good replacement for the $l=0.07\mathrm{H}$ condition. However, attempts to get better agreement with the data of Ueda *et al.* (1977) suggested $C_{\varepsilon F}=3.5$ ($C_{lF}=1.44$ and $\overline{v_n^2}/k=0.546$).

Calculations for infinitely wide open channels were made to reconfirm the choice of C_{lF}. With $C_{lF}=1$, the dissipation length scale becomes 20% too large in comparison to that obtained using the Hossain and Rodi (1980) condition. With $C_{lF}=1.44$, recommended by Yacoub *et al.* (1991), this difference becomes smaller (10%) and the extrapolated length vanishes at 0.09H above the free surface, reconfirming this choice.

Calculations for rectangular open channels with aspect ratios of 1 : 2 and 1 : 4 showed maximum (absolute) values for the lateral stream function that deviate less than 5% from those obtained with the condition of Hossain and Rodi (1980).

2. 6 Free Surface Renewal Conditions for the Pressure-Strain Correlation

The surface renewal model can also be used to estimate C_3 in Equation (23). Here it is suggested that the total amount of energy redistributed due to the open surface proximity :

$$E=\int_0^H 2\left(\frac{\overline{v_n^2}}{k}\right)\varepsilon C_3\,dy \tag{42}$$

is also related to the inward energy flux expected to dissipate by enhanced coherence :

$$E \sim \frac{1}{\rho} J_k = \frac{1}{3}\left(\frac{\overline{v_n^2}}{k}\right)^{3/2} k_s^{3/2} \tag{43}$$

However, with

$$C_3 = C_{3F}^2\left(\frac{1}{y + C_{3F} l}\right)^2 \tag{44}$$

and with constant $k \sim k_s$ and $l \sim l_s$, an approximation for Equation (42) :

$$E = \int_0^H 2\left(\frac{\overline{v_n^2}}{k}\right)\frac{C_\mu^{3/4}}{\kappa}\frac{k^{3/2}}{l} C_{3F}^2\left(\frac{1}{y + C_{3F} l}\right) dy \tag{45}$$

the following is obtained :

$$E \sim 2\left(\frac{\overline{v_n^2}}{k}\right)\frac{C_\mu^{3/4}}{\kappa}\frac{n}{n+1} C_{3F}\, k_s^{3/2} \tag{46}$$

where, $n = H/C_{3F} l_s \simeq 5$. Comparing Equation (46) with Equation (43), an assessment for $C_{3F} \simeq 0.368$ is obtained, reconfirming the choice of Naot and Rodi (1982) of $C_{3F} \simeq 0.316$.

3. COMPUTATIONAL SCHEME

The numerical program STABKY2 is basically a parabolic procedure that solves at each forward step for the seven variables U, V, W, k, ε, P, and ϕ using in the lateral plain an Alternating Direction Implicit (A. D. I.) Algorithm. Three linear momentum equations are solved for the streamwise velocity, W, and the lateral velocities, U and V. Two turbulence model equations are solved for the turbulent energy, k, and the dissipation, ε. The continuity equation is solved for the pressure, P, using the Patankar–Spalding (1972) algorithm. Finally, an equation for the lateral stream function, ϕ, is also solved.

The STABKY2 version is based on the STABLE version restricted to : Cartesian coordinates, straight channel with fixed grid structure, and turbulent flow. New features, however, were introduced : (1) the geometry of the rectangular compound channel, (2) an algebraic stress model, (3) boundary conditions for the dissipation, (4) modifications to the evaluations of the averaged distance from solid walls, and (5) an evaluation of the lateral stream function.

3.1 Lateral Stream Function

Using a vectorial stream function which satisfies the continuity equation, we can decribe the three dimensional flow in the following :

$$U=\frac{\partial \phi_z}{\partial y}-\frac{\partial \phi_y}{\partial z} \tag{47}$$

$$V=\frac{\partial \phi_x}{\partial z}-\frac{\partial \phi_z}{\partial x} \tag{48}$$

and

$$W=\frac{\partial \phi_y}{\partial x}-\frac{\partial \phi_x}{\partial y} \tag{49}.$$

For fully developed flow, however, these equations turn into :

$$U=\frac{\partial \phi}{\partial y}, \quad V=-\frac{\partial \phi}{\partial x} \tag{50}$$

with the scalar lateral stream function ϕ replacing the component ϕ_z. For this case only,

$$\left(\frac{\partial^2}{\partial x^2}+\frac{\partial^2}{\partial y^2}\right)\phi=\frac{\partial U}{\partial y}-\frac{\partial V}{\partial x} \tag{51}.$$

Practically, Equation (51) is iteratively solved along the whole computational process bearing results that are meaningful only towards the fully developed end of the calculation.

3. 2 Averaged Distance from Boundaries

The averaged distance from the external boundaries used in Equation (26) to measure wall proximity is based on the definition of

$$\left\langle\frac{1}{y^2}\right\rangle=\left[\frac{1}{\pi}\int_{-\pi}^{+\pi}\frac{d\theta}{S^2}\right]^{-1/2} \tag{52}$$

where S is the distance to the boundary segment that occupies the angle differential $d\theta$. When a compound channel is considered, the definition is modified so that when S has more than one value, only the smallest value is adopted.

3. 3 Grid Dependence

A set of runs with the ratios $\Delta x/\Delta y=5, 3, 2$, and 1, showed that the intensity of the three lower vortices—two adjacent to the main channel bed and one adjacent to the flood plain left corner—increase with the $\Delta x/\Delta y$ ratio decrease. The intensity of the other four upper vortices, however, decreases. This mainly affects the zone of maximum streamwise velocity which is dipped by the second current well below the free surface, e. g., the velocity –dip phenomenon, (see Nezu and Nakagawa 1992). To restrict the errors in the prediction of the secondary currents within five percent, it is not recommended to allow for $\Delta x/\Delta y>$ 1.25. Therefore, $\Delta x=\Delta y$ was used here.

A refinement of the grid is also associated with the reduction of y_1^+ at the first grid node where the wall functions are used. The present choice of a 24×120 grid restricts $65<y_1^+<100$ for $Re=10^5$. Further refinement is not recommended because y_1^+ should be set as $y_1^+\geq50$, as pointed out by Nezu and Nakagawa (1987).

3.4 Convergence and Fully Developed Flow

Convergence was identified by means of the cumulative absolute values of the mass sources summed for the 2880 grid cells. A typical plot of this, versus the forward step in a logarithmic paper, indicates three phenomena : a high peak is shown at about 200 steps ($z=12H$) presumably due to the mass displacement from the developing boundary layers. A second, smaller peak is shown at about 1500 steps ($z=90H$) presumably due to the secondary currents imposing their relative importance in the convecting mass. The third phenomenon is a strong oscillation presumably due to the sensitivity of the A. D. I. algorithm to poor precision. To dispense with this, using the Fujitsu M-385 computer, a double precision procedure was needed. To reduce the mass sources to 10^{-6}, the step size was reduced. 3000 steps were used, with a single iteration at each step, for a calculation that was terminated at $z=182H$ for $Re=10^5$. Observing the slow variation with a forward step indicated that fully developed conditions were established. This was reconfirmed by observing the negligible sensitivity to the initial turbulence energy level.

The calculations were performed with a homogeneous grid with 24×120 internal nodes (regular cells). Typical double-precision calculations with 3000 forward steps, consumed approximately 25 minutes CPU time on the Fujitsu M-385. The streamwise distance reached depends on the Reynolds number $Re_H\equiv H\langle W\rangle/\nu$:

$$z/H=182(Re_H/10^5)^{0.25} \tag{53}$$

based on an analogy with the distance needed for the development of an identical boundary layer thickness using Blasius formula. For $Re_H=3.162\times10^4$, 10^5, 10^6, and 10^7, the distances : $z/H=136$, 182, 323, and 574 were considered, respectively.

4. THE COMPOUND RECTANGULAR OPEN CHANNEL

The basic hydrodynamic features : the streamwise velocity contours, the lateral streamlines, the energy of turbulence, and the wall shear stress distribution are given for the four configurations shown in Fig. 2 ; (a) the asymmetric smooth channel, (b) the symmetric smooth channel, (c) the wide symmetric smooth channel, and (d) the asymmetric smooth channel with rough flood plain.

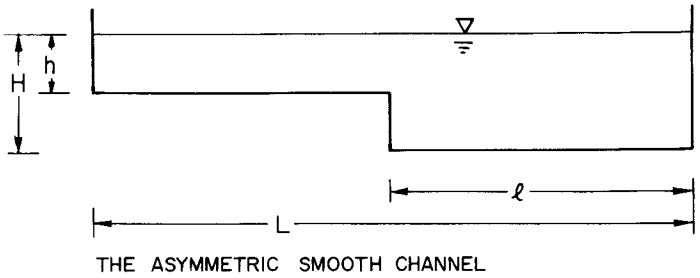

THE ASYMMETRIC SMOOTH CHANNEL

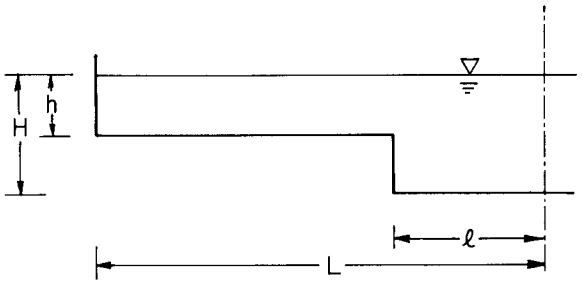

THE SYMMETRIC SMOOTH CHANNEL

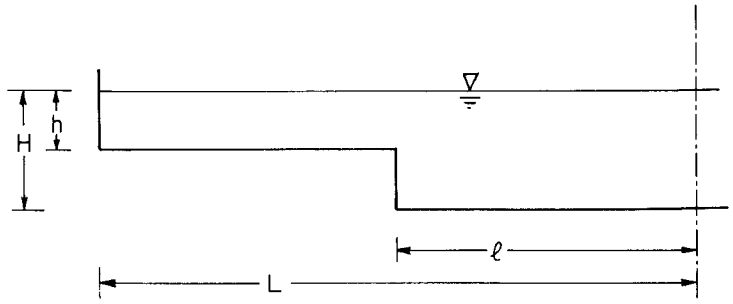

THE WIDE SYMMETRIC CHANNEL

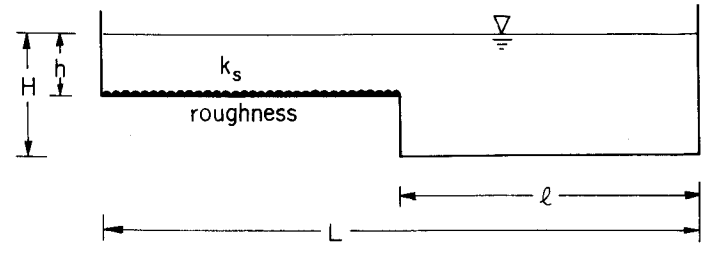

ASYMMETRIC CHANNEL WITH ROUGH FLOOD PLAIN

Fig. 2 The Compound Open-Channel Flow Configurations.

4.1 The Asymmetric Compound Smooth Open Channel

The calculated results shown here refer to the three test cases S-1, S-2, and S-3 measured by Tominaga and Nezu (1991) with $l/L=0.5$, $H/L=0.20$, and $h/H=0.25$, 0.50, and 0.75, respectively. Streamwise velocity contours are shown in Fig. 3. The primary mean velocity W is normalized by its maximum velocity W_{max}. With an increase in the flood plain depth the drift of the maximum streamwise velocity below the free surface due to the secondary currents becomes less pronounced. In a deep flood plain, however, a second zone of maxium streamwise velocity is formed. The agreement of these two trends with the experiments of Tominaga and Nezu (1991) is well reasonable. To explain these trends, one should note the lateral streamlines shown in Fig. 4. The stream function ϕ is normalized by the flow depth H and the primary bulk velocity $\langle W\rangle$ averaged in the cross section. With an increase in the flood plain depth the intensity of the vortices in the main channel decreases, while the intensity of the vortex at the flood plain increases.

Fig. 5 shows the contour lines of turbulent energy $k/\langle U_*^2\rangle$ normalized by the averaged friction velocity $\langle U_*\rangle$. They indicate the maximum values along the main channel bed and banks, and minimum values close to the free surface. With an increase in the flood plain depth, the energy of turbulence at the flood plain bed increases till it equals the level at the main channel bed. Comparison with the experimental data of Tominaga and Nezu (1991)

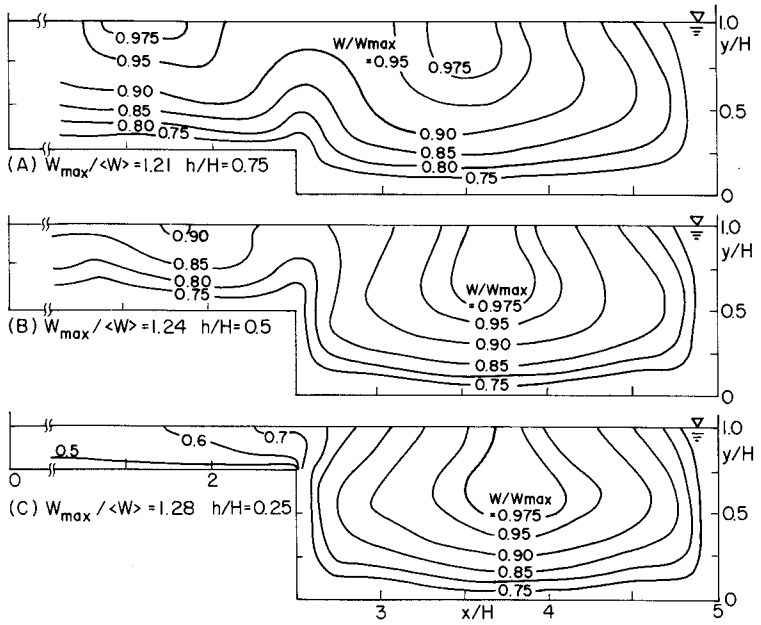

Fig. 3 Streamwise Velocity Contours, W/W_{max}, for $Re_H=10^5$ in the Asymmetric Smooth Channel.

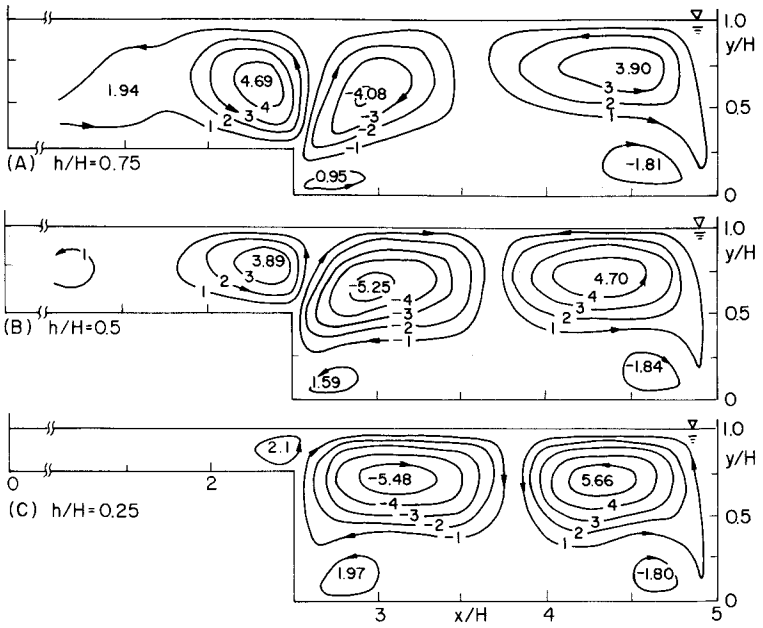

Fig. 4 Lateral Stream Function, $10^3\phi/\langle W\rangle H$, for $Re_H=10^5$ in the Asymmetric Smooth Channel.

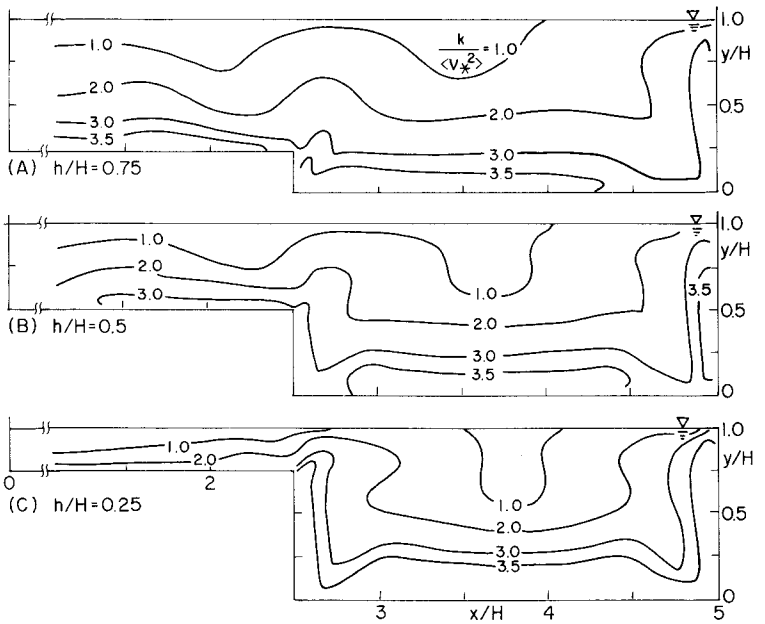

Fig. 5 Energy of Turbulence, $k/\langle U_*^2\rangle$, for $Re_H=10^5$ in the Asymmetric Smooth Channel.

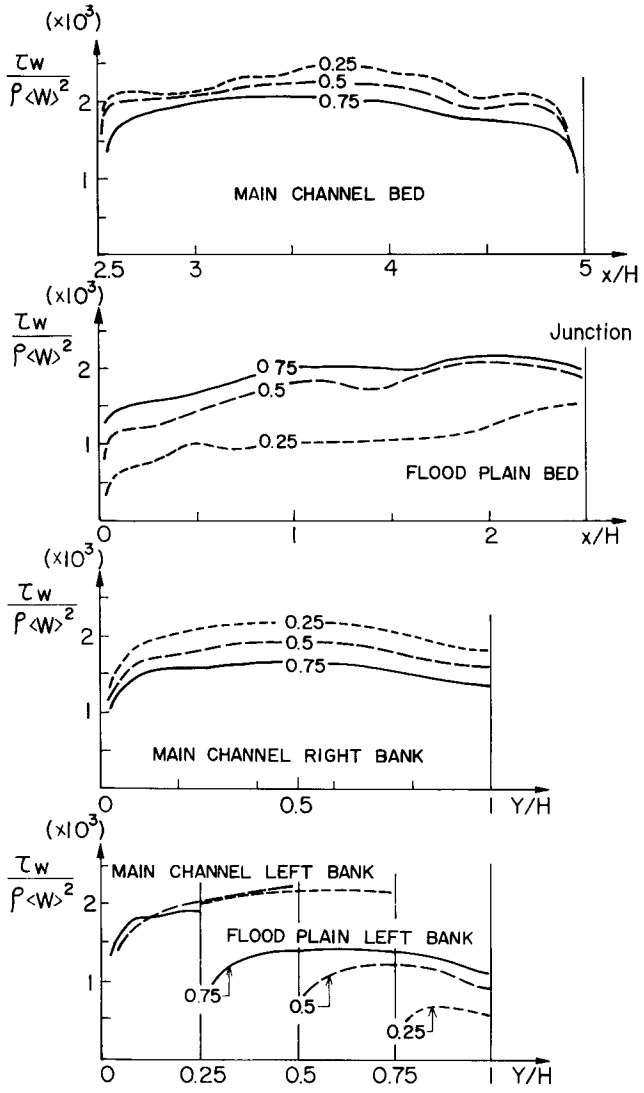

Fig. 6 Wall Shear Stress, $10^3\tau_\omega/\rho\langle W\rangle^2$, for $Re_H=10^5$ in the Asymmetric Smooth Channel.

for the case of $h/H=0.5$ shows reasonable qualitative agreement. The calculated values, however, are somewhat smaller, typical of the 'standard' choice of the model coefficients adopted here.

The local shear stress distribution, shown in Fig. 6, shows opposite trends with an increase in the flood plain depth. The local shear stress at the main channel bed and the right

bank somewhat decrease, and the local shear stress at the flood plain bed and left bank increase considerably. Only the left bank of the main channel is almost unaffected. Comparison with the experimental data of Tominaga and Nezu (1991), using $\langle U_*^2 \rangle / \langle W \rangle^2 = 1.76 \times 10^{-3}$, 1.83×10^{-3} and 1.73×10^{-3} for the $h/H = 0.75$, 0.5, and 0.25 cases respectively, shows reasonable agreement.

4.2 The Symmetric Smooth Channel

Three symmetric compound channels are discussed. Here, the flood plain and the main channel dimensions are the same as used by Tominaga and Nezu (1991). However, due to

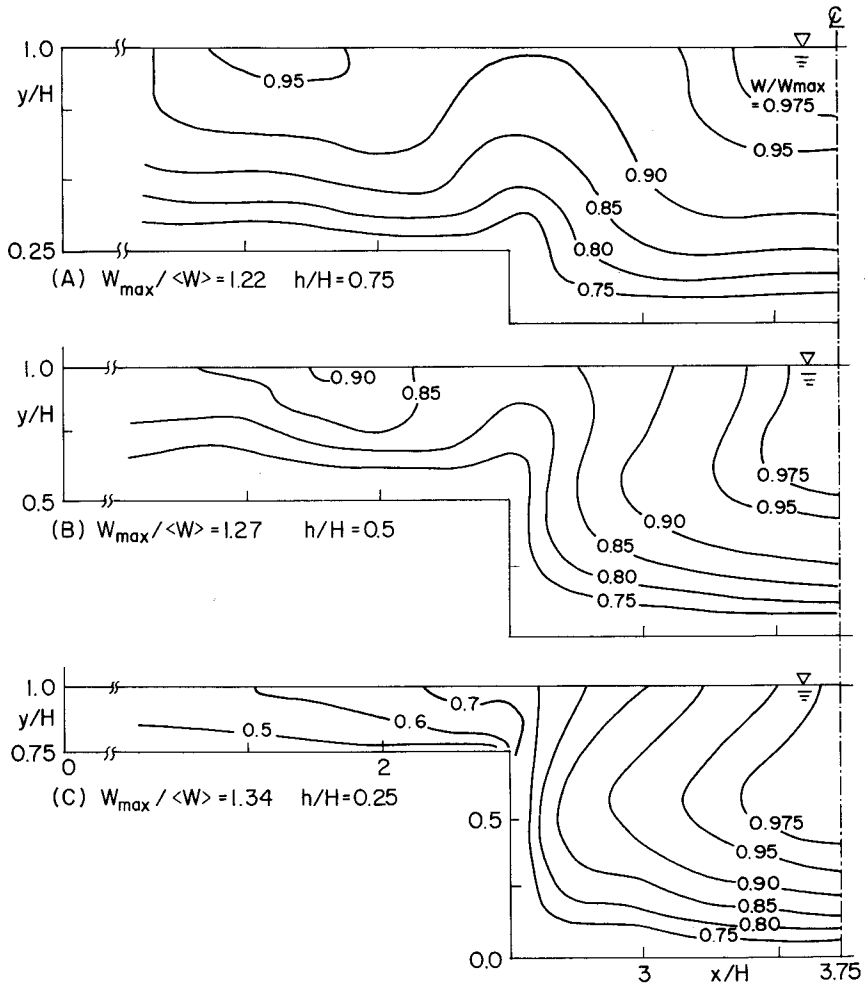

Fig. 7 Streamwise Velocity Contours, W/W_{max}, for $Re_H = 10^5$ in the Symmetric Smooth Channel.

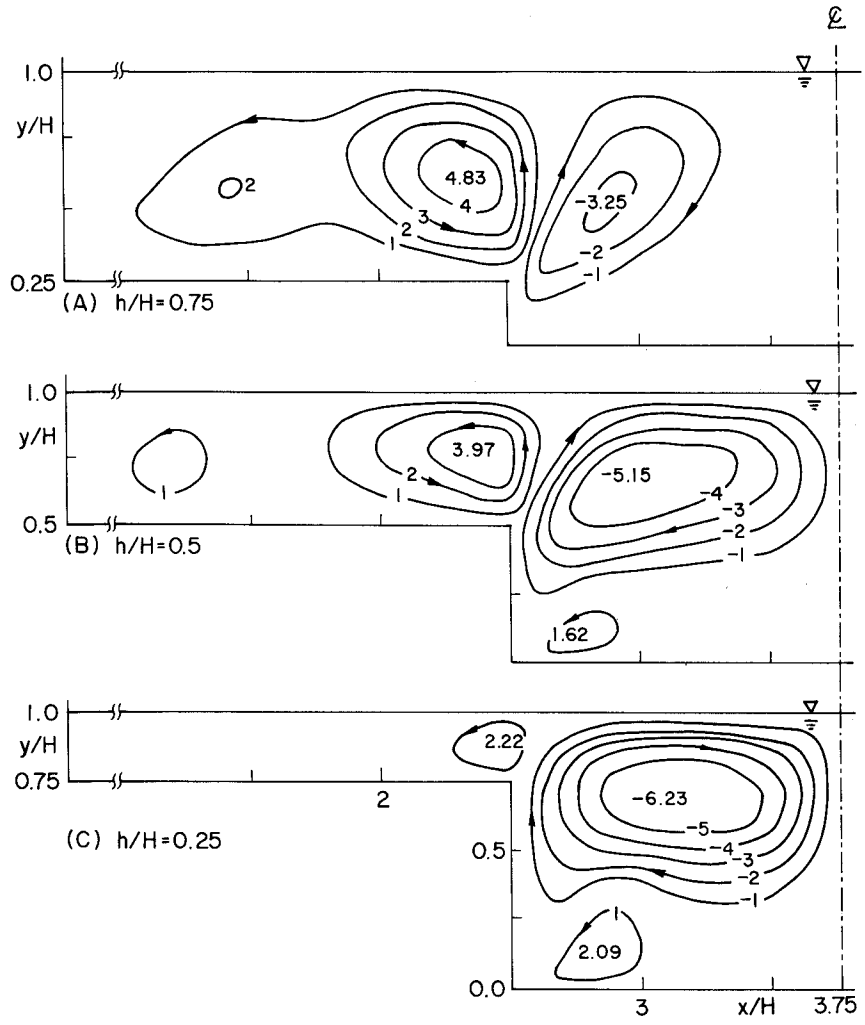

Fig. 8 Lateral Stream Function, $10^3\phi/\langle W\rangle H$, for $Re_H=10^5$ in the Symmetric Smooth Channel.

the symmetry, the proportion between the flood plains and the main channel cross section areas was doubled with respect to the reference cases. Calculations were performed for $H/L=0.2667$, $l/L=0.3333$, and $h/H=0.25$, 0.50, and 0.75 (see Fig. 2).

The streamwise velocity contours shown in Fig. 7 and the lateral stream lines shown in Fig. 8 should be compared to those shown in Fig. 3 and Fig. 4, respectively, for the asymmetric channels. As the flow depth h/H of the flood plain increases, the intensity of the vortex in the flood plain increases and the vortex in the main channel becomes weaker.

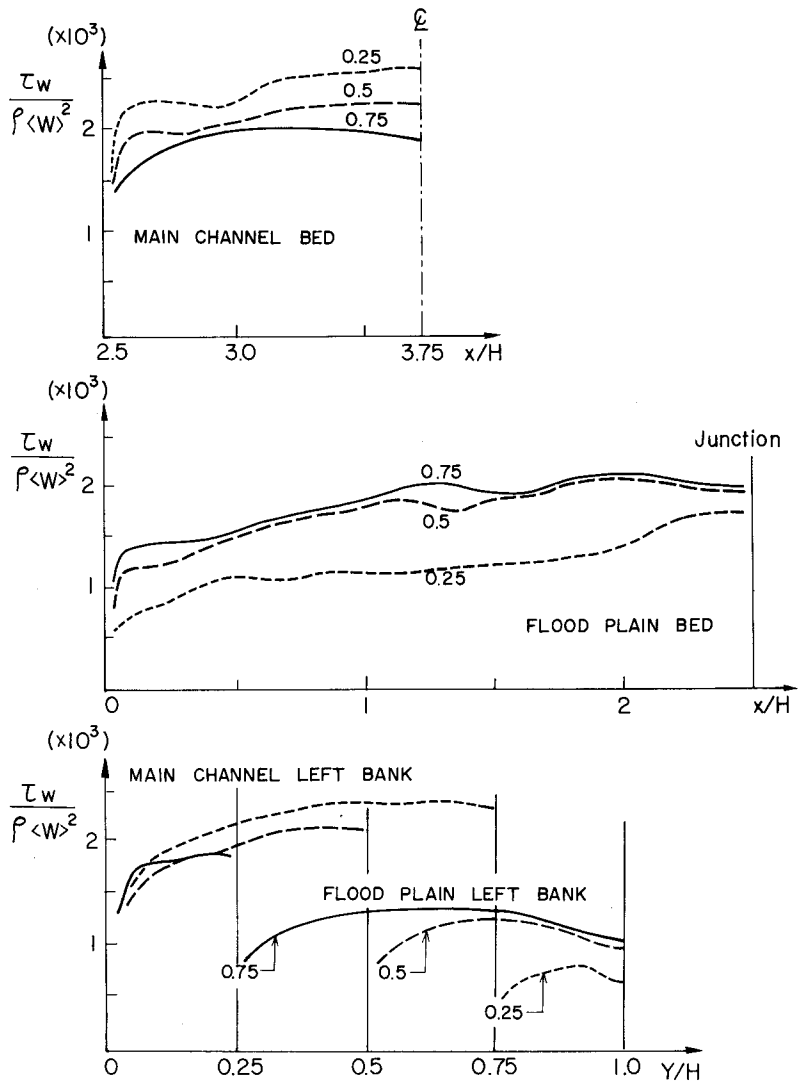

Fig. 9 Wall Shear Stress, $10^3\tau_\omega/\rho\langle W\rangle^2$, for $Re_H=10^5$ in the Symmetric Smooth Channel.

These opposite trends at the main channel show up in the streamwise velocity contours, mainly in the drift of the zone of maximum velocity by lateral motion. Basically, the local shear stress distribution for the symmetric cases shown in Fig. 9 is similar to that shown for asymmetric cases in Fig. 6. Only for the shallow flood plain, $h/H=0.25$, an increase in the stresses at the main channel bed and bank shows up.

4. 3 The Wide Symmetric Channel

Three symmetric compound channels with the same proportion between the flood plains and the main channel cross sections as practised by Tominaga and Nezu (1991) are now discussed. Here, the main channel width is doubled with respect to the reference cases. Calculations were performed for $H/L=5.0$, $l/L=0.50$ and $h/H=0.25$, 0.50 and 0.75 (see Fig. 2).

Streamwise velocity contours are shown in Fig. 10. Due to the increased main channel width, the drift of the zone of maximum velocity below the free surface is not effective even for the shallow flood plain, and the formation of a second zone of maximum streamwise velocity at the deep flood plain is less pronounced.

The lateral stream lines shown in Fig. 11 show a reduction in the vortex intensity due to the increase in the channel width. The calculations also predict a new vortex which is in fact an extension of the small vortex at the bottom of the left corner of the main channel.

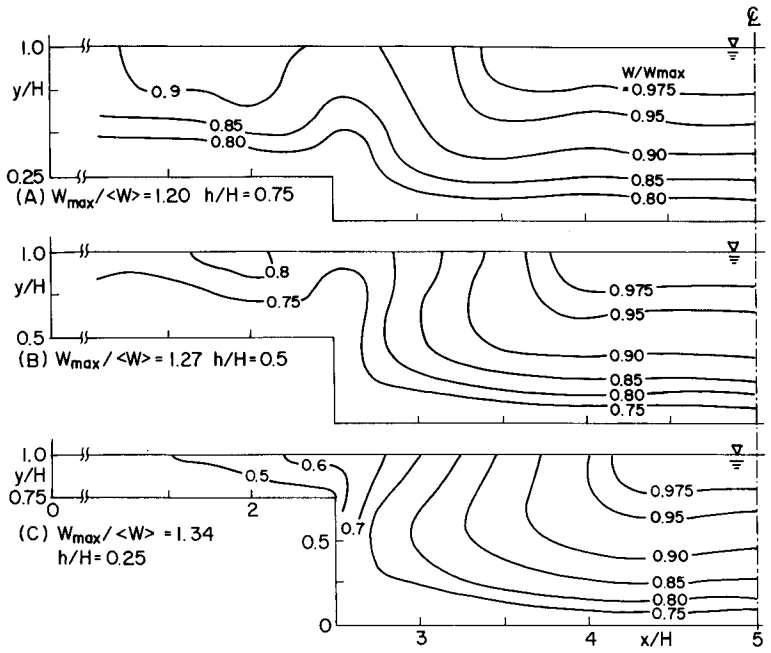

Fig. 10 Streamwise Velocity Contours, W/W_{max}, for $Re_H=10^5$ in the Symmetric Wide Channel.

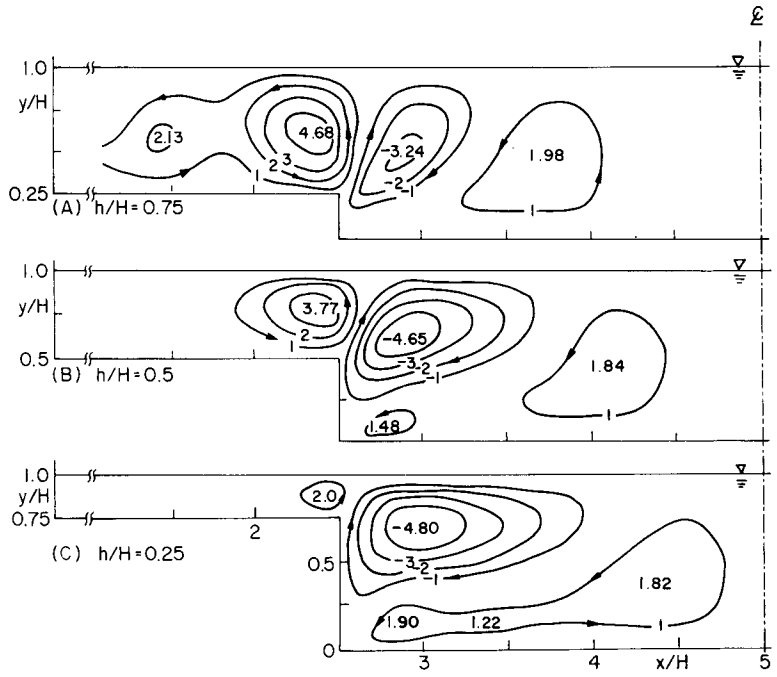

Fig. 11 Lateral Stream Function, $10^3\phi/\langle W\rangle H$, for $Re_H=10^5$ in the Symmetric Wide Channel.

4.4 The Asymmetric Channel with Rough Flood Plain

Three simulations were performed in order to study the effects of the flood-plain roughness on the basic hydrodynamic features. These were performed for $Re_H=10^5$, $l/L=0.5$, $H/L=0.2$, and $h/H=0.5$ with the equivalent sand roughness height of $k_s/H=0.006$, 0.012, and 0.024. The last study corresponds to the case R-1 measured by Tominaga and Nezu (1991). The option for rough surface wall function was activated with equivalent sand height 'plus', k_s^+, being close to the lower bound of the complete rough regime; $k_s/H=0.006$, 0.012 and 0.024 correspond to $88<k_s^+<127$, $94<k_s^+<135$, and $100<k_s^+<154$, respectively.

In Fig. 12 the basic features: the streamwise velocity contours, W/W_{max}, the lateral stream lines, $\phi/(\langle W\rangle H)$, and the energy of turbulence, $k/\langle U_*^2\rangle$, are shown for the case with $k_s/H=0.024$. This flood-plain roughness enhances the following aspects: a decrease of about 15 percent in the streamwise velocity in the flood plain, an increase of about 74 percent in the intensity of the vortex hanging over the flood plain, and an increase of about 43 percent in the turbulence energy adjacent to the flood plain bed.

The wall shear stress distribution is shown in Fig. 13. With an increase in the flood plain bed roughness, a large increase of about 100 percent in the flood plain bed shear stress

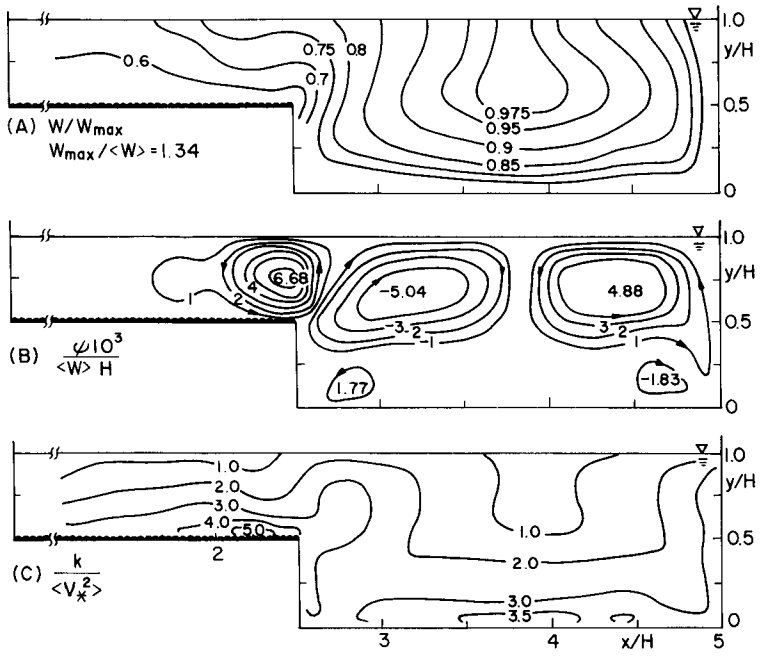

Fig. 12 The Asymmetric Channel with Rough Flood Plain Features: (A) W/W_{max}, (B) $10^3\psi/\langle W\rangle H$, and (C) $k/\langle U_*^2\rangle$. ($Re_H=10^5$, $k_s/H=0.024$, $h/H=0.5$).

is observed. This is accompanied by a small increase of about 20 percent in the main channel shear stress, but the wall shear stress at the flood plain left bank decreases by about 43 percent. While the first effect is directly due to the surface roughness, the second two effects stem from the mass transferred from the flood plain to the main channel; compare the vortex strength over the flood plain of Fig. 12 with that of Fig. 4.

5. THE HYDRODYNAMIC BEHAVIOUR OF THE COMPOUND OPEN CHANNEL

The hydrodynamic behaviour of the compound open channel is demonstrated by showing the dependence of a few overall flow parameters on the Reynolds number, the flood plain depth, the symmetry of the channel, and the flood plain roughness. The averaged wall shear stress, the continuous mass exchange between the flood plain and the main channel, and the mass displacement from the flood plain to the main channel, are discussed in the following.

5.1 Reynolds Number Effects

Probably the best way to realize the effects of an increase in the Reynolds number is

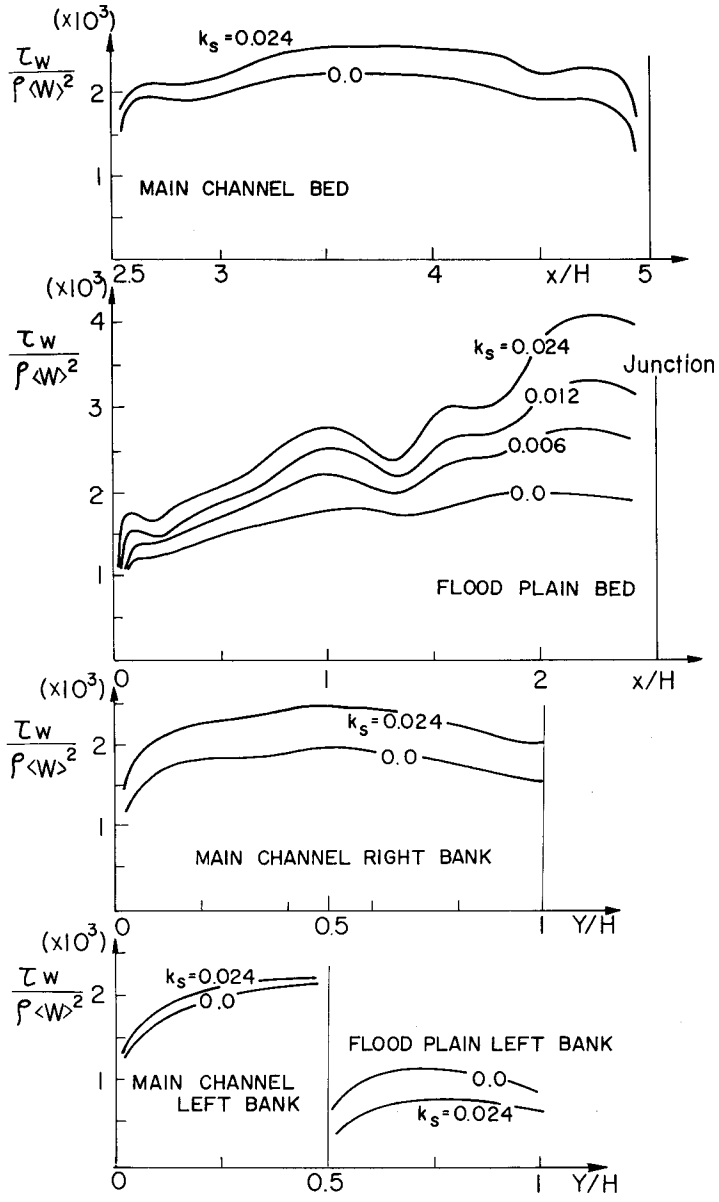

Fig. 13 Wall Shear Stress, $10^3\tau_\omega/(\rho\langle W\rangle^2)$, for $Re_H=10^5$ in the Asymmetric Channel with Rough Flood Plain.

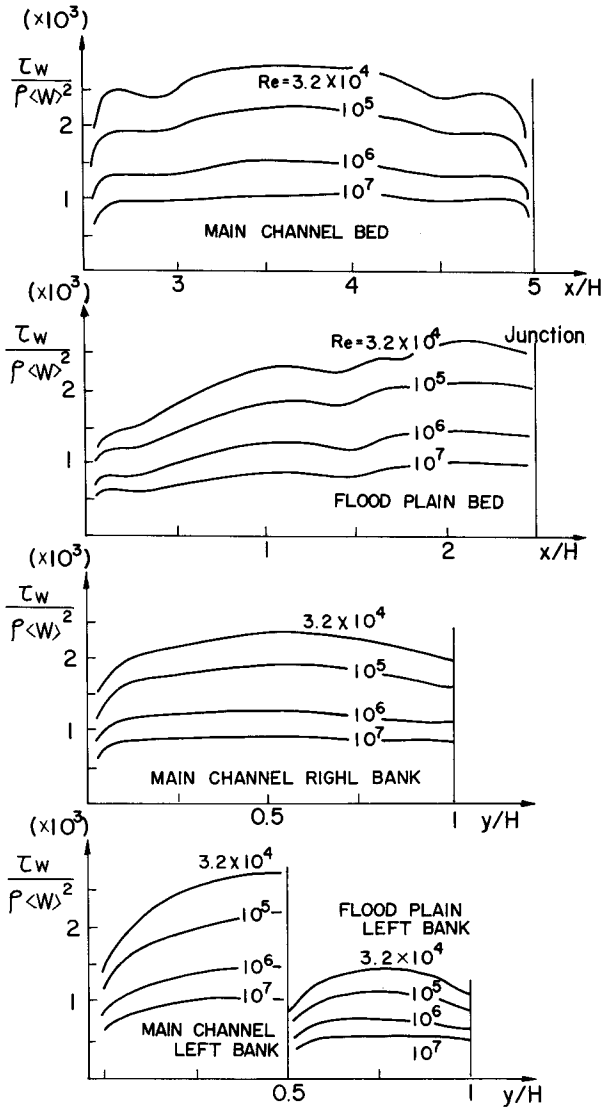

Fig. 14 Dependence of the Asymmetric Smooth Channel Wall Shear Stress, $10^3\tau_\omega/\rho\langle W\rangle^2$, on the Reynolds Number.

made by observing that the local wall shear stress, shown in Fig. 14, becomes uniform and that the waves due to the secondary currents disappear. Above $Re_H=10^8$, the secondary currents lose their importance and the assumption of uniform shear stress becomes plausible.

The overall effect is shown by means of the friction factor. Since $\partial\phi^*/\partial z$ in Equation

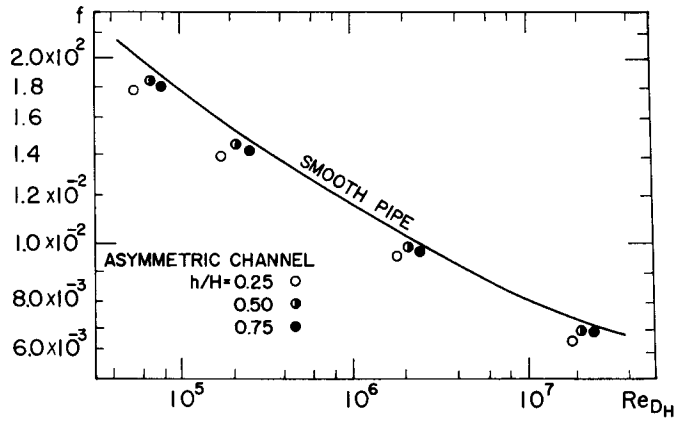

Fig. 15 Dependence of the Asymmetric Smooth Channel Friction Factor, f, on the Reynolds Number, Re_{D_H}.

(6) becomes equal to $\rho g \sin\theta$ at the fully developed end of the calculations, a friction factor f can be defined :

$$f \equiv I_e D_H / (\langle W \rangle^2 / 2g) = 2g \sin\theta \, D_H / \langle W \rangle^2 \tag{54}$$

It is shown that f is equal to $8\langle U_*^2 \rangle / \langle W \rangle^2$.

The value of f was calculated directly from the program output and the results are given in Fig. 15 on the background of a Moody diagram for smooth round pipe flow ; the friction factor, f, versus the Reynolds number, $Re_{D_H} \equiv D_H \langle W \rangle / \nu$.

5. 2 Friction Factors

The dependence of the friction factors on the flood plain depth for the asymmetric and the symmetric compound channels is shown in Fig. 16. To explain these trends we note that the overall friction factor $f = 8\langle \tau_w \rangle / \rho \langle W \rangle^2$ is related to the averaged shear stress :

$$\langle \tau_w \rangle = \sum_{i=1} \tau_{w_i} \Delta S_i / S \tag{55}$$

where τ_{w_i} is the averaged shear stress in a sub-channel, ΔS_i is the sub-channel wetted perimeter, and S is the total wetted perimeter. Using the sub-friction factors $f_i = 8\tau_{w_i} / \rho \langle W \rangle_i^2$ we obtain :

$$f = \sum_{i=1} f_i (\Delta S_i / S) (\langle W \rangle_i / \langle W \rangle)^2 \tag{56}$$

Considering the flood plain as sub-channel 1 and the main channel as sub-channel 2,

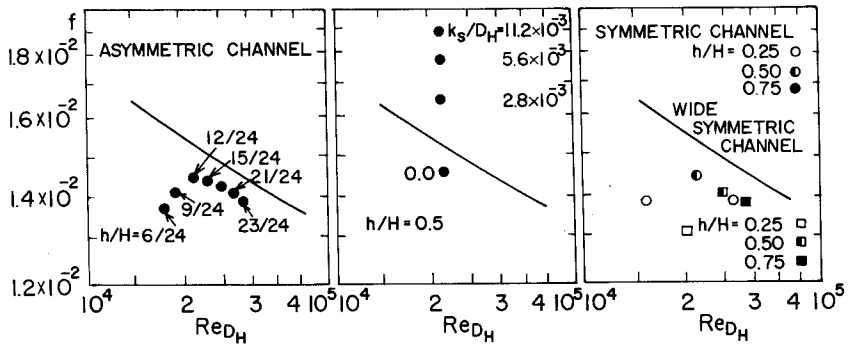

Fig. 16 Dependence of the Friction Factor, f, on the Flood Plain Depth, h/H, and the Roughness, k_s/D_H, for the Main Channel Symmetry and Width.

the ratio $\langle W\rangle_2/\langle W\rangle$ becomes a unit for small $\langle W\rangle_1/\langle W\rangle$ typical of small h/H, and f becomes $f_2\,\Delta S_2/S$ which is smaller than f_2, typical of the main channel by a factor that may reach 0.643 for vanishing h/H. A decrease in f with a decrease in h/H ratio is therefore expected.

The effects of the flood plain roughness are also shown in Fig. 16. To explain these trends, we rewrite Equation (56) as:

$$f \simeq 0.154 f_1 + 0.823 f_2 \tag{57}$$

for the approximation: $\Delta S_1/S=3/7$, $\Delta S_2/S=4/7$, $\langle W\rangle_1/\langle W\rangle=0.6$ and $\langle W\rangle_2/\langle W\rangle=1.2$. Using an estimation for $f_2 \simeq 0.0146$, we obtain for the rough flood plain sub-channel:

$$f_1 \simeq 0.0441,\ 0.0367,\ \text{and}\ 0.0294 \tag{58}$$

using the calculated values $f=0.0188$, 0.0177, and 0.0165. These values for f_1 indeed correspond to our expectations for channels with $k_s/D_H=0.0112$, 0.0056, and 0.0028, respectively.

5.3 Continuous Mass Exchange Between Flood Plain and Main Channel

Attention is focused here on the intensity of the vortex hanging over the flood plain threshold as it represents the continous mass exchange between the flood plain interior and the main channel. To calculate this mass flow rate, in m^2/sec, one has to multiply the reported values for the maximum stream function by $10^{-3}\langle W\rangle h$. The dependence on the Reynolds number, shown in Fig. 17, suggests slow decrease with an increase of the Reynolds number, Re_{D_H}. The dependence on the flood plain depth is shown in Fig. 18, for the asymmetric and the symmetric channels, and for the channel with a rough flood plain. The

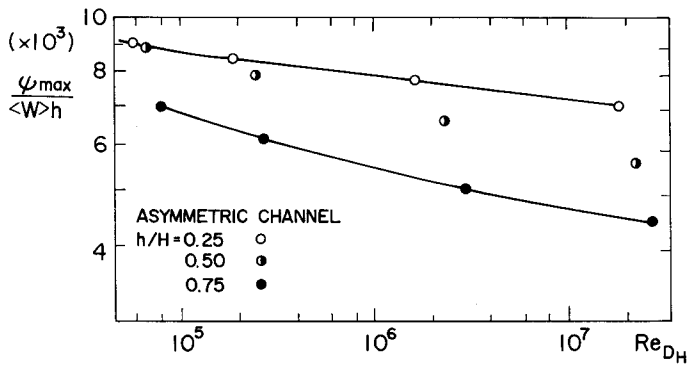

Fig. 17 Dependence of the Vortex Pair Intensity, $10^3\phi_{max}/(\langle W\rangle h)$, at the Flood Plain Threshold on the Reynolds Number, Re_{D_H}.

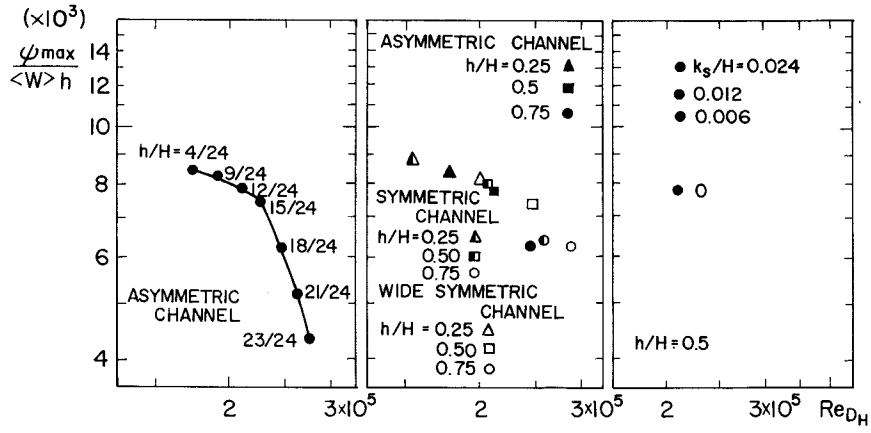

Fig. 18 Dependence of the Vortex Pair Intensity on the Flood Plain Depth and Roughness, and also on the Main Channel Symmetry and Width.

relative rate $\phi_{max}/h\langle W\rangle$ decreases considerably with an increase of the flood plain depth and increases considerably with an increase of the flood plain roughness.

5.4 Mass Displacement

With the streamwise advance of the calculation, the ratios $W_{max}/\langle W\rangle$ within the two sub channels of the flood plain and the main channel increase, indicating mass displacement from the boundary layers into the sub channels interior. The fact that the maximum value for the main channel is larger than that of the flood plain suggests that mass is shifted from the flood plain to the main channel.

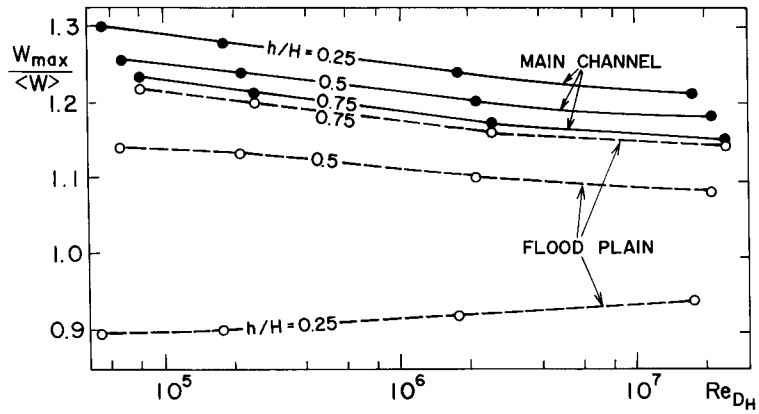

Fig. 19 Dependence of the Maximum Streamwise Velocity, $W_{max}/\langle W\rangle$, in the Main Channel and the Flood Plain on the Reynolds Number, Re_{D_H}.

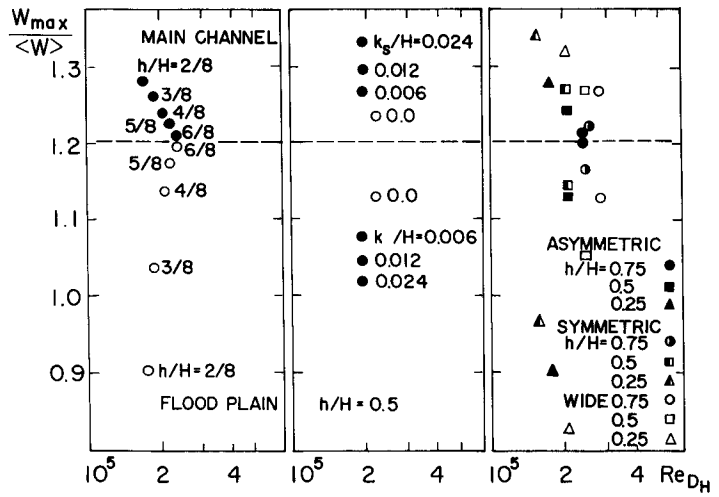

Fig. 20 Dependence of Subchannel Streamwise Velocity Maxima on the Flood Plain Depth and Roughness, and also on the Main Channel Symmetry and Width.

The values of $W_{max}/\langle W\rangle$ are given in Fig. 19 in terms of the Reynolds number, Re_{D_H}. With the Reynolds number increase, these values tend to become united, indicating that the flow within the sub channels becomes uniform and that the overall mass displacement from the flood plain to the main channel decreases.

The dependence of $W_{max}/\langle W\rangle$ on the flood plain depth and the roughness is shown in Fig. 20. For the deep flood plain, $h/H > 5/8$, the difference between the main channel and

the flood plain vanishes, indicating that the still high displacement rate from the boundary layers is not accompanied by mass displacement between the two sub channels. For small h/H, however, and for the rough flood plain, a large difference is found, indicating intensive mass displacement from the flood plain to the main channel.

6. MISCELLANEOUS ASPECTS OF OPEN CHANNEL FLOW

Three topics typical of the compound open channel flow are discussed in the following. The importance of the special coherent structure typical of the flood plain threshold for the modelling of the flow is clarified. A cellular structure induced by a low flood plain threshold is shown. Finally, a cellular structure induced by the interactions of the turbulent eddies with the open surface is demonstrated, suggesting a possible explanation for the formation of the multi-cellular structure.

6.1 Coherent Structure at the Flood Plain Threshold

The corner formed at the flood plain entrance from the main channel, here referred to as the "flood plain threshold", is characterized by eight-shaped [8] vortices with periodic path-line intersections (Tamai, Asaeda and Ikeda, 1986). Obviously this coherent structure affects the two point velocity correlations, and thus its structure makes the quasi-isotropic models of Naot, Shavit and Wolfshtein (1973) and Launder, Reece and Rodi (1975) inadequate. However, the comparison of vector plots indicates that the errors in the prediction of the lateral mean velocity are small, less than 5 percent, in spite of this theoretical weakness.

6.2 Low Flood Plain Threshold

Results for a small difference between the plain depth and the main channel depth $h/H=0.958$, which still maintain the main flow characteristics, are shown in Fig. 21. In spite of the low threshold height, the streamwise velocity contours show two separated zones of maximum velocity, and the lateral streamlines show an almost symmetric intensive vortex pair at the bed discontinuity. The wall shear stress is also given in Fig. 21. It is indicated that a small misalignment between two adjacent channel bed segments of a few percents of the channnel depth may form a vortex cell that is of similar structure and intensity as that reported by Nezu and Nakagawa (1984) and Nezu *et al.* (1985) for multi-cellular structure in closed channels, and also by Nezu and Nakagawa (1989) for multi-cellular structure in fluvial open channels. It is plausible that longitudinal ridges produce a similar flow pattern.

6.3 Enhancement of Cellular Structure by the Free Surface

The interactions of the turbulent eddies adjacent to the free surface are modeled by a boundary condition for the dissipation rate ε and a special redistribution term of turbulent

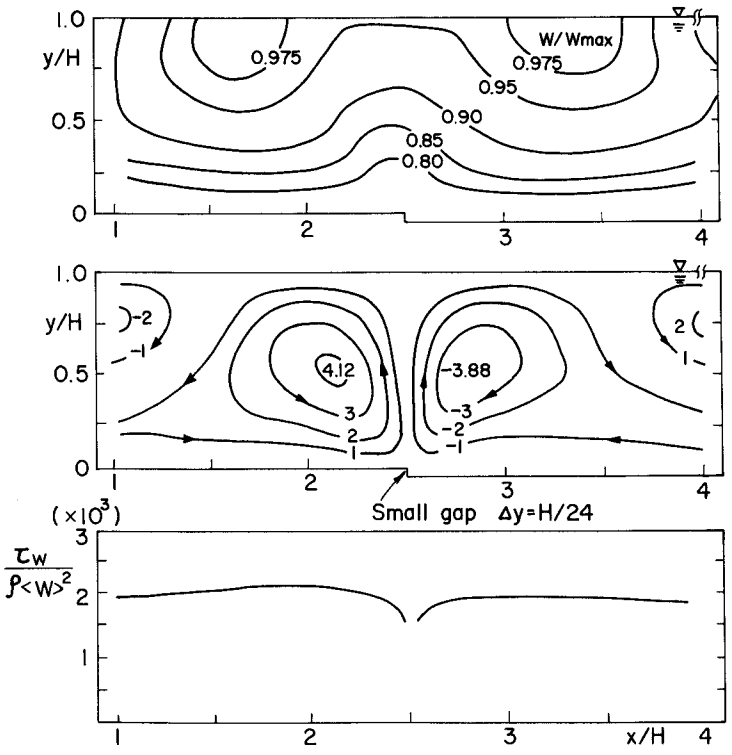

Fig. 21 The Low Flood-Plain Height Features: W/W_{max}, $10^3\phi/\langle W\rangle H$, and $10^3\tau_\omega/\rho\langle W\rangle^2$. $W_{max}/\langle W\rangle = 1.20$ and $h/H = 23/24$.

energy. An important argument leading to the models is an expected coherence leading to a high collision rate. The possibility that these interactions also depend on the lateral flow direction led to an experiment with C_3 reduced considerably (0.33) in free surface segments. Indeed, cellular structure was obtained showing an intensity weaker ($\phi_{max} \simeq 0.87\ 10^{-3}\langle W\rangle H$) than that measured by Nezu and Nakagawa (1991). Note, however, that the measurements in a sand free laboratory channel of Imamoto, Ishigaki and Nishida (1989) show weak lateral motion. We may suggest that the onset of the multi-cellular structure is due to the free surface interactions, later augmented and stabilized by sand or sediment ridges built up at the urban channel bed (Nezu et al, 1989).

7. CONCLUDING REMARKS

The potentiality of the relatively simple algebraic stress model of Naot and Rodi (1982), in describing the basic hydrodynamic features of the rectangular compound open channel,

was demonstrated.

The application of the flux boundary condition for the dissipation at the free surface was found a useful tool for an open channel with variable depth. It was shown that the model coefficient of the redistribution term typical of the free surface proximity can be related to the coefficient of the flux condition for the dissipation, forming a comprehensive model for the free surface renewal process.

Two main trends with the Reynolds-number increase were shown. The local shear stress tends to become uniform towards the Reynolds number $Re_H = 10^8$. The maximum values of the vortex pair that determine the mass transfer from the flood plain to the main channel, when normalized using $\langle W \rangle h$, are slightly affected by the Reyolds-number increase.

The present algebraic stress model is based on a quasi-isotropic concept and therefore cannot cope with the special coherent structure typical of the flood plain threshold. Still, the errors in calculating the momentum equations for the ambiant fluid are limited. However, this may have a more pronounced effect when sediment transport is considered, as it determines the transfer rate within the vortex pair at the flood plain threshold.

Finally, some clues to the origin of the multi-cellular structure typical of the wide open channel were also given, suggesting that the free-surface induced turbulent interactions may be the origin of a weak cellular structure which is later augmented and stabilized by the formation of sand ridges.

ACKNOWLEDGEMENTS

The computer code was adjusted at the Center for Technological Education, Holon, Israel, and the research was performed at the Division of Global Environment Engineering, Graduate School of Engineering, Kyoto University, Kyoto, Japan, where the first author stayed as a guest professor. The financial support was awarded by "The Kyoto University Foundation". These support of institutions and the devoted help of Mr. Zuckermann, Mrs. Davidovich of the CTE-Holon, Dr. Hosada, Mr. Murase and Mr. Ishida of Kyoto University as well as Prof. A. Tominaga of Nagoya Institute of technology is hereby acknowledged.

REFERENCES

1. Gessner, F. B. and A. F. Emery, "The Numerical Prediction of Developing Turbulent Flow in Rectangular Ducts", *Proceedings: Turbulent Shear Flows 2*, London, England, (1979).
2. Hossain, M. S. and W. Rodi, "Mathematical Modelling of Vertical Mixing in Stratified Channel Flow", *Proceedings of the 2nd Symposium on Stratified Flows*, Trondheim, Norway, (1980).
3. Imamoto, H., T. Ishigaki and M. Nishida, "Turbulence, Secondary Flow and Boundary Shear Stress in a Trapezoidal Open Channel", *23rd Congress of IAHR.*, Vol. A., pp. 23-30, Ottawa, Canada, (1989).

4. Launder, B. E., G. J. Reece, and W. Rodi, "Progress in the Development of a Reynolds Stress Turbulence Closure", *Journal of Fluid Mechanics*, Vol. 68, pp. 537–566, (1975).
5. Launder B. E. and D. B. Spalding, "The Numerical Computation of Turbulent Flow", *Computer Methods in Applied Mechanics and Engineering*, Vol. 3, pp. 269–289, (1974).
6. Launder, B. E. and W. M. Ying, "Prediction of Flow and Heat Transfer in Ducts of Square Cross Section", *Proceedings, Institution of Mechanical Engineers*, Vol. 187, pp. 455–461, (1973).
7. Naot, D. and S. Emrani, "Numerical Simulation of the Hydrodynamic Behaviour of Fuel Rods with Longitudinal Cooling Fins", *Nuclear Engineering and Design*, Vol. 73, pp. 319–329, (1983).
8. Naot, D. and W. Rodi, "Applicability of Algebraic Models Based on Unidirectional Flow to Duct Flow with Lateral Motion", *International Journal of Numerical Methods in Fluids*, Vol. 1, pp. 225–235, (1981).
9. Naot, D. and W. Rodi, "Calculation of Secondary Currents in Channel Flow", *Journal of the Hydraulics Division*, ASCE, Vol. 108, pp. 948–968, (1982).
10. Naot, D. and W. Rodi, "Interaction of the Turbulent Eddies with Free Surface", *Liquid Metal Flow and Magnetohydrodynamics* (eds. H. Branover, P. S. Lykoudis and A. Yakhot), Progress in Astronautics and Aeronautics, Vol. 84, AIAA, Inc., 1633 Broadway, New York, (1983).
11. Naot, D., A. Shavit, and M. Wolfshtein, "Numerical Calculation of Reynolds Stresses in a Square Duct with Secondary Flow", *Wärme-und-Stoffübertragung*, Vol. 7, No. 3, pp. 151–161, (1974).
12. Neti, S. and R. Eichhorn, "Computation of Developing Turbulent Flow in a Square Duct", *Turbulent Boundary Layers* (ed. H. E. Weber), ASME, New York, (1979).
13. Nezu, I. and H. Nakagawa, "Cellular Secondary Currents in Straight Conduit", *Journal of Hydraulic Engineering*, ASCE, vol. 110, pp. 173–193, (1984).
14. Nezu, I. and H. Nakagawa, "Numerical Calculation of Turbulent Open-Channel Flows in Consideration of Free-Surface Effect", *Memoirs of Faculty of Engineering*, Kyoto University, vol. 49, No. 2, pp. 111–145, (1987).
15. Nezu, I. and H. Nakagawa, "Self Forming Mechanism of Longitudinal Sand Ridges and Troughs in Fluvial Open Channel Flow", *23rd Congress of IAHR*, Vol. B., pp. 65–72, Ottawa, Canada, (1989).
16. Nezu, I. and H. Nakagawa, "Three Dimensional Structure of Turbulence and the Associated Secondary Currents in Urban Rivers", *Environmental Hydraulics* (*eds. J. H. W. Lee & Y. K. Cheung*), Balkema Publishers, vol. 1, pp. 379–384, (1991).
17. Nezu, I. and H. Nakagawa, "*Turbulence in Open-Channel Flows*", IAHR-monograph, Balkema Publishers, Rotterdom, (1992).
18. Nezu, I., H. Nakagawa, M. Mitsunari, and N. Kawashima, "Measurements of Cellular Secondary Currents and Sand Ribbons in Fluvial Open Channel Flows", *Proceedings of the 4th Osaka Symposium on Flow Measuring Techniques*, pp. 9–24, Osaka, Japan, (1989).
19. Nezu, I., H. Nakagawa and A. Tominaga, "Secondary Currents in a Straight Channel Flow and the Relation to its Aspect Ratio", *Turbulent Shear Flows 4*, Springer-Verlag, vol. 4, pp. 246–260, (1985).
20. Nezu, I. and W. Rodi, "Experimental Study on Secondary Currents in Open Channel Flow", *Proceedings of 21st Congress of IAHR*, vol. 2, pp. 115–119, Melbourne, Australia, (1985).
21. Nezu, I. and W. Rodi, "Open-Channel Flow Measurements with a Laser Doppler Anemometer", *Journal of Hydraulic Engineering*, ASCE, vol. 112, pp. 335–355, (1986).

22. Nikuradse : H. Schlichting *"Boundary Layer Theory"* (4th ed.), McGraw-Hill, New York, p. 523, (1960).
23. Patankar, S. V. and D. B. Spalding, "Calculation Procedure for Heat Mass and Momentum Transfer in Three-Dimensional Flows", *International Journal of Heat and Mass Transfer*, Vol. 15, pp. 1787-1806, (1972).
24. Reece, G. J., "*A Generalized Reynolds Stress Model of Turbulence*", Thesis presented to the University of London, England, in partial fulfillment of the requirements for the degree of Doctor of Philosophy, (1976).
25. Shir, C. C., "A Preliminary Numerical Study of Atmospheric Turbulent Flows in the Idealized Planetary Boundary Layer", *Journal of Atmospheric Science*, Vol. 30, pp. 1327-1339, (1973).
26. Tamai, N., T. Asaeda, and H. Ikeda, "Generation Mechanism and Periodicity of Large Surface Eddies in a Compound Channel Flow", 5th Congress of the Asian and Pacific Division of IAHR, Vol. 2, pp. 61-74, Seoul, Korea, (1986).
27. Tatchell, D. G., "*Convective Processes in Confined Three Dimensional Boundary Layers*", Thesis presented to Imperial College, London, England, in partial fulfillment of the requirements for the degree of Doctor of Philosophy, (1975).
28. Tominaga, A., I. Nezu, and S. Kobatake, "Flow Measurements in Compound Channels with a Fiber Optic Laser Doppler Anemometer", *IAHR workshop on Instrumentation for Hydraulics Laboratories*, pp. 45-59, Canada Centre for Inland Waters, Burlington, Canada, (1989).
29. Tominaga, A. and I. Nezu, "Turbulent Structure in Compound Open Channel Flows", *Journal of Hydraulic Engineering*, ASCE, Vol. 117, pp. 21-41, (1991).
30. Ueda, H., R. Möller, S. Komori, and T. Mizushina, "Eddy Diffusivity Near the Free Surface of Open Channel Flow", *International Journal of Heat and Mass Transfer*, Vol. 20, pp. 1127-1136, (1977).
31. Yacoub, N., D. Moalem Maron, and D. Naot, "Towards the Numerical Simulation of the Horizontal Slag Front", *International Journal for Numerical Methods in Fluids*, Vol. 13, (1991).